Angewandte Chemie
Eine Zeitschrift der Gesellschaft Deutscher Chemiker

Supporting Information

69451 Weinheim, Germany

Hofmeister Salts Recover a Misfolded Multiprotein Complex for Subsequent Structural Measurements in the Gas Phase**

*Linjie Han and Brandon T. Ruotolo**

anie_201301893_sm_miscellaneous_information.pdf

Materials and Methods

Materials **-** Concanavalin A tetramer (ConA, jack bean), and all salts studied including cations (acetate anion with tetramethylammonium (TMA), sodium, potassium, rubidium, lithium, Tris (2-Amino-2-hydroxymethyl-propane-1,3-diol), calcium, barium, and magnesium counterions) or anions (ammonium cation with fluoride, chloride, nitrate, tartrate, hydrogen phosphate, sulfate and perchlorate counter-ions) were purchased from Sigma (St. Louis, MO, USA). All other chemicals used in this study were analytical quality, and all aqueous solutions were prepared on the Synergy water purification system (Millipore Corporation).

Ion Mobility-Mass Spectrometry (IM-MS) **-** Typically, a sample aliquot (~5 µL) was analyzed using a quadrupole-ion mobility-time-of-flight mass spectrometry (Q-IM-ToF MS) instrument (Synapt G2 HDMS, Waters, Milford MA, USA)[1]. Concanavalin A tetramer (ConA) was first buffer exchanged into 100 mM ammonium acetate at pH 7 using Micro Bio-Spin 6 columns (Bio-Rad, Hercules, CA) and prepared to a final concentration of 5 µM. ConA' was refolded by adding small amounts of salt in solution prior to nESI, where the identity of cations (acetate anion with tetramethylammonium (TMA), sodium, potassium, rubidium, lithium, Tris (2-Amino-2-hydroxymethyl-propane-1,3-diol), calcium, barium, and magnesium counterions) or anions (ammonium cation with fluoride, chloride, nitrate, tartrate, hydrogen phosphate, sulfate and perchlorate counter-ions) were altered specifically so that their effect could be evaluated individually. All salts were prepared as stock solutions in 100 mM ammonium acetate at a concentration of 20mM, before addition to the protein solution, where the final salt concentration was 2 mM. The total salt and protein concentrations listed above were chosen primarily to avoid nESI-based ion suppression effects.[2] Protein ions were generated using a nESI source in the positive mode, with the capillary typically held at 1.5 kV. The sample cone was operated at 50 V. Instrument settings were optimized to allow transmission of intact protein complexes and to preserve non-covalent interactions[3]. The trap traveling-wave ion guide was pressurized to 3.3×10^{-2} mbar of argon gas. The ion trap was operated in an accumulation mode and ion lifetimes in the trap prior to IM analysis range from 0-50 ms in our experiments. The traveling-wave ion mobility separator was operated at a pressure of ~ 3.5 mbar, and employed a series of DC voltage waves (40 V wave height traveling at 600-1000 m/s) to generate ion mobility separation. The ToF-MS was operated over the m/z range of 400–8000 and at a pressure of 1.6×10^{-6} mbar.

Mass spectra were calibrated externally using a solution of cesium iodide (100 mg ml^{-1}) and processed with Masslynx 4.1 software (Waters, UK). Collision cross-section (CCS) measurements were made using

known CCS values of transthyretin (TTR), avidin, alcohol dehydrogenase (ADH), and glutamine dehydrogenase (GDH) tetramers (Sigma-Aldrich), as calibrants using the method described previously[4].

Collision Induced Unfolding (CIU) and Dissociation (CID) - CIU 'fingerprints' for ConA and ConA' were generated through collisional activation in the ion trap traveling-wave ion guide prior to the ion mobility separator in tandem-MS (Quad selection) mode. Selected ions had a m/z corresponding to the 21^+ of ConA and ConA' and were activated by increasing the trap collision voltage (Trap CE, as indicated in the instrument control software) which acts as a bias voltage between the quadrupole and ion trap traveling-wave ion guide to accelerate ions to increased kinetic energies for CIU experiments. The energy-dependent arrival-time distribution profiles (CIU 'fingerprints') were constructed using 5 V step-wise increments in trap CE. In addition, post IM separation CID of 20^+ protein complex ions for ConA and ConA' was performed in the 'transfer' traveling wave ion guide in order to analyze and compare the charge state distributions of monomeric product ions.

Circular Dichroism (CD) - The CD spectra were measured with an Aviv model 202 CD spectrometer (Aviv Instruments, Lakewood, USA). A 1-mm-path-length quartz cuvette was used for scanning between 205 and 250 nm. The concentration of ConA tetramer was 5 µM.

Differential Scanning Calorimetry (DSC) - The DSC experiments were performed on Nano DSC (TA Instruments, New Castle, USA). The concentration of ConA tetramer was 6.0 mg/mL, equivalent to ~ 60 µM. The measurements were performed at temperatures from 45 to 95 °C at a scan rate of 2 °C/min. The reference solution in all the calorimetric experiments was 100 mM ammonium acetate and all samples were degassed before measurement. The DSC data were fit with two-state scaled model by using the software NanoAnalyze (TA Instrument, USA) to obtain the temperature (T_m) at which maximum heat exchange occurs.

Comparison of ConA and ConA' MS data (Figure S1) - We are able to isolate the MS data corresponding to only ConA and ConA' (Figure S1) using careful control of solution conditions and spectral post-processing. We observe an increase in average charge state for tetrameric ConA' (red) relative to ConA (black), indicated by higher signal intensity corresponding to the 21^+ charge state and a new 22^+ peak. This increase in average charge correlates well with our increased CCS measurements (ConA' has a 12% larger CCS than ConA). The charging of intact protein complexes by nESI is known to be dependent upon protein surface area, and simple estimates of this attribute based on CCS allow us to predict an increase of ~1 charge for ConA' relative to ConA based on literature data.[5]

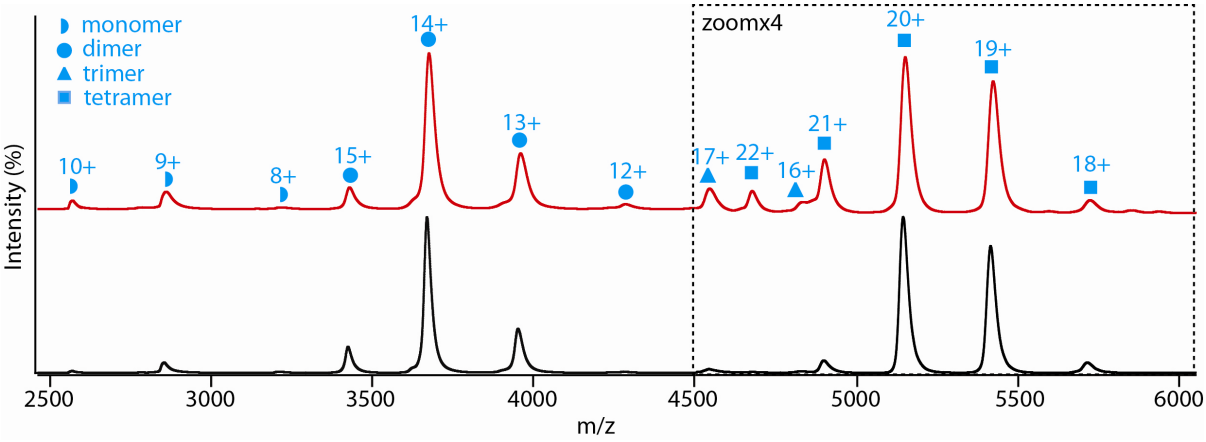

Figure S1. Mass spectra of ConA obtained from nESI solutions prepared using control (100 mM ammonium acetate) conditions (black) and following multiple freeze-thaw cycles (red). The charge states are indicated for tetramers (square), trimers (triangle), dimers (circle) and monomers (half circle). The spectra are magnified 4 fold above 4500 m/z.

Verifying the assignment of ConA' as a misfolded form of ConA tetramer through solution-phase disruption (Figure S2, S3 and S4) **-** To probe the origin of ConA', we endeavored to structurally characterize its subcomplexes and subunits. It should be noted that ConA can exist as tetramer, dimer and monomer under all solution compositions tested herein. Small amounts of other forms such as trimer and hexamer are believed to arise from the nonspecific interactions formed during the ESI process. Figure S2 exhibits the controlled distortion of native state ConA by dissolving it into 100 mM ammonium acetate solutions containing 20% (vol/vol) glacial acetic acid (pH = 5.2) and 0%-30% (vol/vol) methanol. In this weakly-acidic solution, the ConA tetramer evolves from a native-like form (black dotted line) to a structure having longer drift times (red dotted line) as the fraction of methanol is raised (Figure S2A). This new conformer has a similar CCS to the ConA' formed following several freeze-thaw cycles, thus we refer to both similarly, and this feature dominates the 21^+ of ConA tetrameric ions when

the methanol volume fraction reaches 20%. In addition, the 10^+ ion of ConA monomer undergoes significant conformational changes with increasing methanol concentration (Figure S2C) while there is no significant change for the 15^+ ConA dimer (Figure S2B).

To further study ConA' structure, the complex was dissolved into 100 mM ammonium acetate solutions containing 0%-50% (vol/vol) methanol (Figure S3) and 0%-60% (vol/vol) DMSO (Figure S4), which are polar protic and aprotic solvents respectively. A greater population of ConA’ is produced as the volume fraction of methanol is increased, whereas the CCS observed for DMSO containing solutions remains virtually unchanged from the value expected for 'native-like' ConA. We note that the tetramer size is observed to increase (by ~1%) in a manner correlated with DMSO addition, but we do not observe any production of ConA’ at any DMSO solvent fraction. Larger amounts of methanol (>50%) or DMSO (>60%) are required to completely deplete the tetramers observed (data not shown).

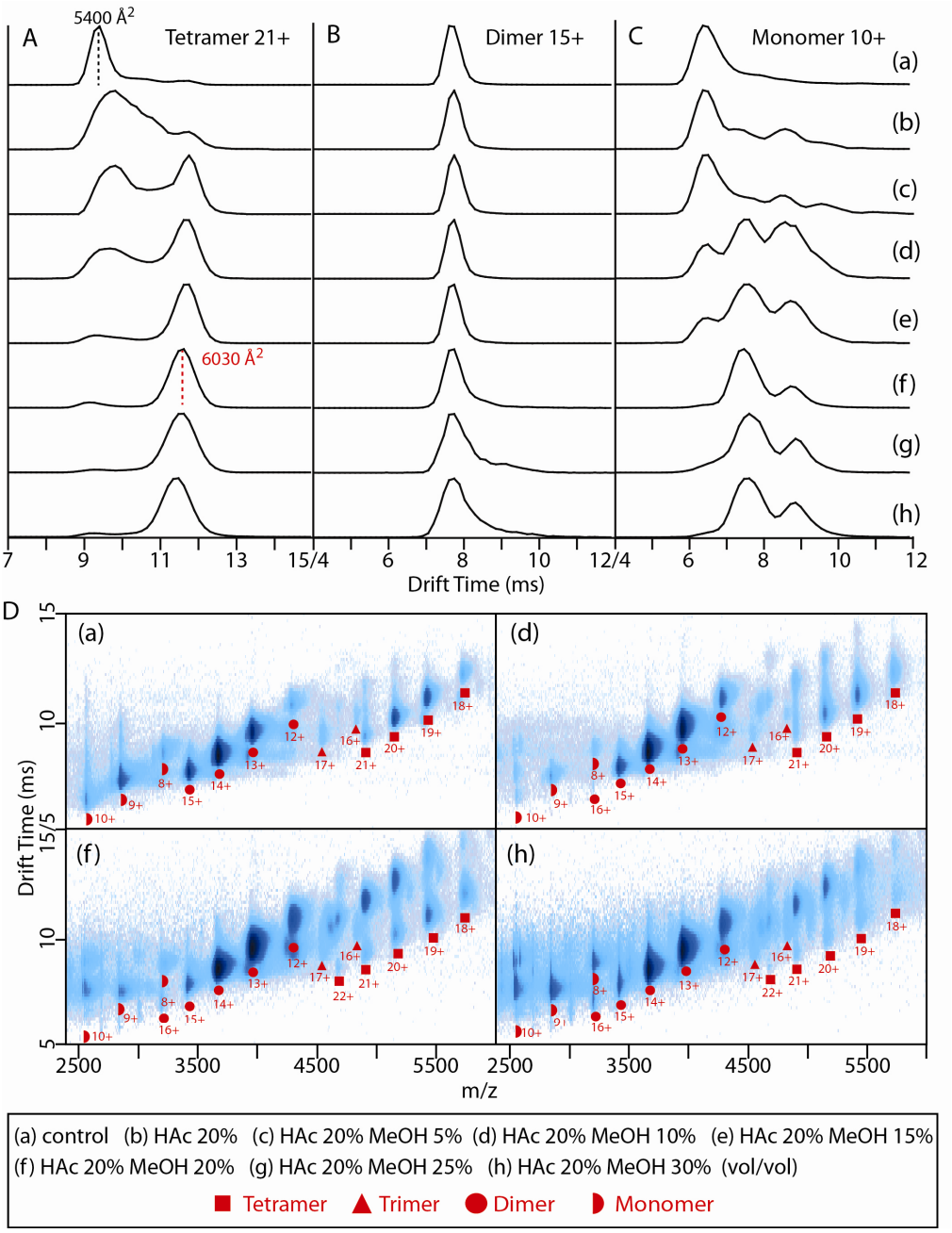

Figure S2. Controlled distortion of native-like ConA (control in solution (a) containing 100 mM ammonium acetate) by 7 different acetic acid (HAc):methanol (MeOH) solutions (b to h). **(A), (B) and (C)** show the drift time distributions measured for the 21^+ charge state of ConA tetramer, 15^+ of dimer and 10^+ of monomer in 8 different solution compositions, respectively. The 20%:20% HAc: MeOH was selected for use in Figure S5, S6, S7 and S8. **(D)** Drift time versus m/z contour plots obtained for ConA/ConA' ions formed from 4 solution compositions (a, d, f and h). Trimers observed here most likely result from the nonspecific interaction of monomer and dimer during the ESI process.

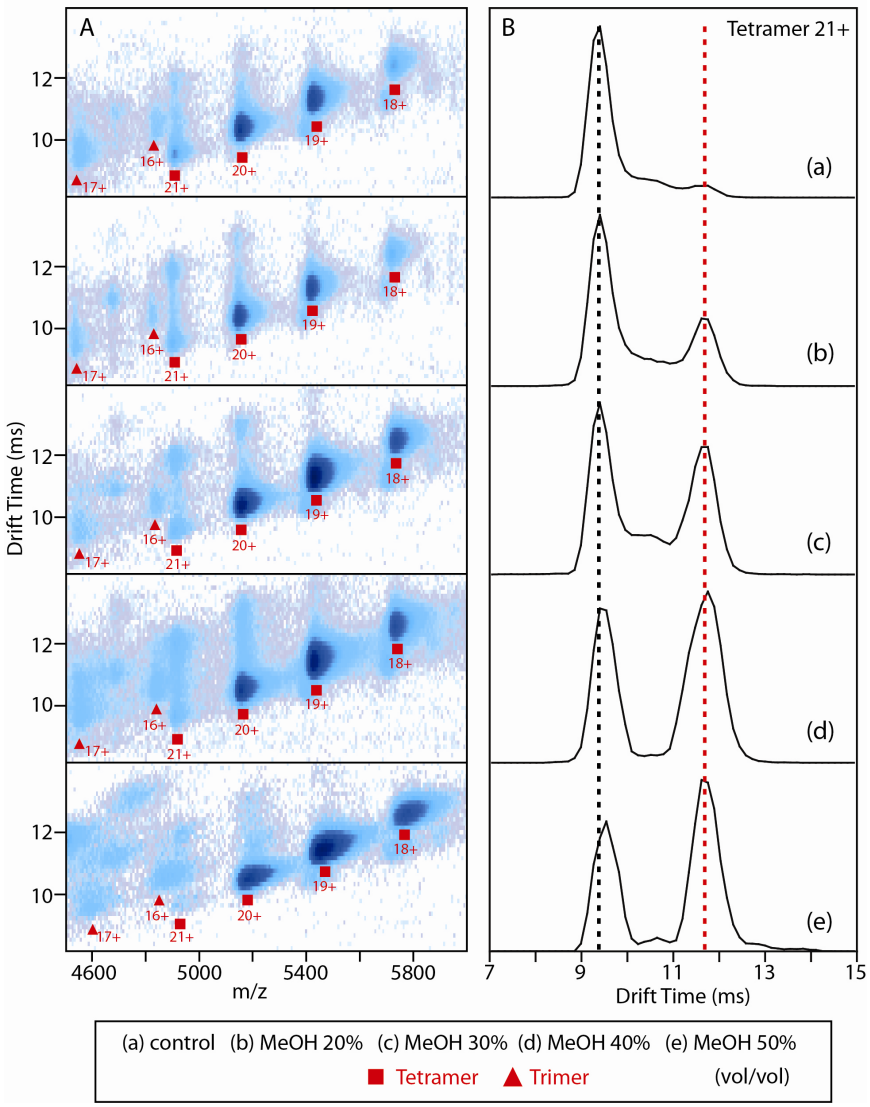

Figure S3. Controlled distortion of ConA (control in solution (a) containing 100 mM ammonium acetate) by 4 different MeOH fractions in aqueous solution (b to e). **(A)** Drift time versus m/z contour plots obtained for ConA/ConA' tetramer ions formed from 5 solution compositions (as indicated). **(B)** Drift time distributions measured for 21^+ charge state of ConA tetramer, from the 5 solution compositions shown in A. The increase in the methanol fraction progressively produces a greater population of ConA' (red dashed line) relative to ConA (black dashed line).

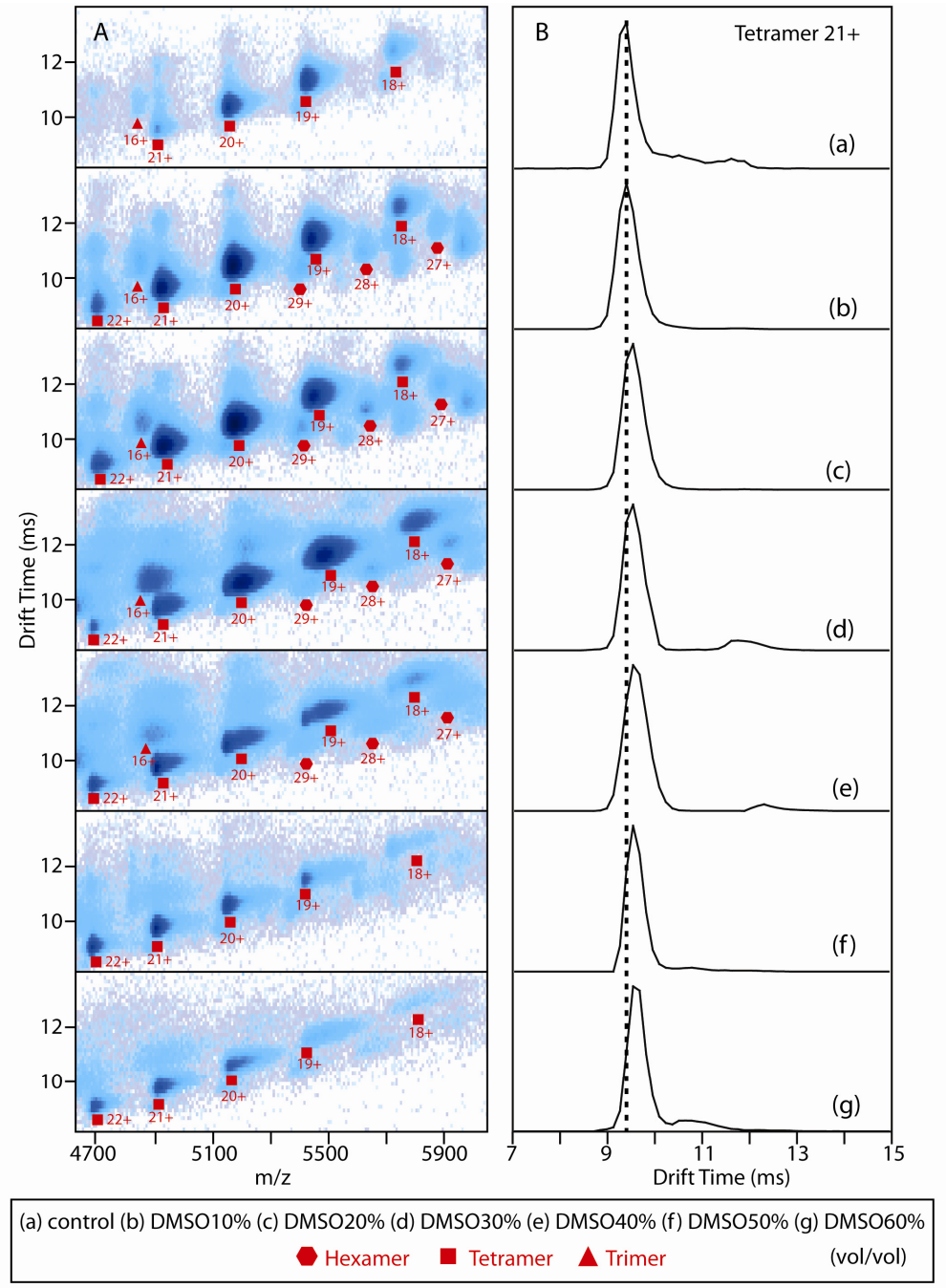

Figure S4. Controlled distortion of ConA (control in solution (a) containing 100 mM ammonium acetate) using 6 different aqueous solvent compositions having varying amounts of dimethyl sulfoxide (DMSO) (b to g). **(A)** Drift time versus m/z contour plots obtained for ConA tetramer ions formed from different DMSO solution compositions. Small signals for nESI artifact trimers and hexamers can also be observed. Additionally, DMSO results in slight supercharging of ConA tetramer where 22^+ charge state is observed, which can be attributed largely to surface tension effects[6]. **(B)** Drift time distributions measured for the 21^+ charge state of the ConA tetramer measured from the solution compositions indicated. A slight

increase in ConA CCS is observed (1%), in a manner correlated with the increased fraction of DMSO used as a solvent.

Probing the origins of ConA' in solution using circular dichroism and differential scanning calorimetry (Detailed discussion of Figure 2) – To probe the solution structure of ConA under conditions that mimic those used for our nESI-IM-MS samples, we performed CD and DSC measurements. Figure 2A shows the far-UV CD spectra between 250-205 nm for ConA in the presence of different amounts (% v/v) of methanol at pH 7. Native ConA exhibits a band at 223 nm (black curve, 100 mM ammonium acetate control), which is characteristic of proteins dominated by β-sheet character[7]. When ConA is prepared in 100 mM ammonium acetate solutions containing varying amounts of (vol/vol) methanol, we observe a red shift of ~4 nm in combination with a decrease in ellipticity, indicative of ConA structure disruption (green curve). We observe that solutions containing greater than 40% added methanol dramatically reduces CD absorptivity. This result strongly correlates with our IM-MS data that shows evidence of ConA' formation at similar methanol concentrations (Figure S3). We also observe similar CD signals at lower methanol amounts (10-30%) upon acidification of ConA containing solutions (Figure 3B), which also agrees with IM-MS results (Figure S2). Due to the large far-UV absorptivity of DMSO, and related chemical noise, CD data from such solutions was not collected.

In addition to CD, we also measured the thermal stability of ConA tetramer by means of DSC (Figure 2C). Due to the boiling point of methanol (65 °C), methanol-containing samples were buffer exchanged following incubation times sufficient to alter ConA structure, prior to DSC measurements. Data for ConA tetramer prepared in 100 mM ammonium acetate alone reveals two thermal unfolding transitions (control). The high temperature transition peak has a T_m of ~85 °C, which agrees with that of native ConA previously reported[8]. The lower temperature transition peak (T_m: ~78 °C) likely corresponds to a small amount of ConA dimer in solution, which co-exists with the tetramer under such solution conditions. After incubation in 10% methanol in a weakly acidic solution, ConA undergoes a significant shift in thermal stability (T_m: ~67 °C). Increasing methanol content to 20% further destabilizes ConA (~55 °C). In sharp contrast to these results, the addition of 10%-20% DMSO to ConA solution has no influence on protein stability, in good agreement with IM-MS data (Figure S4).

Confirmation of the ConA' assignment as a misfolded form of ConA through collisional activation (Figure S5) - Additional insight into the structure of ConA' can be obtained through collisional activation. Using IM-MS, we can construct a 'CIU fingerprint' for 21^+ of ConA (Figure S5A) and ConA' generated by incubating ConA in a 20%:20% acetic acid:methanol solution (Figure S5B)[9]. Both ConA and ConA' occupy the same number of intermediate unfolded conformations, beginning from the most compact conformer (I and I') having a ~12% difference in CCS, and reaching a similar maximally-unfolded conformation (IV and IV') having a shared CCS value of 7550 $Å^2$. Post-IM CID was also performed on ConA and ConA' in ion transfer which sits after the ion mobility cell. In this sense, the dissociated products (monomers and fragments) bear the same drift time as their precursor tetrameric ions. These data are shown in Figure S5C, and we observe that monomeric product ions produced from ConA' exhibit lower charge states (6^+ and 7^+) than those produced from ConA. This result also points to a potential difference in structure between the monomers that comprise the tetramer quaternary structures observed, consistent with the data shown in Figure S2. The mass difference measured between ConA and ConA' (Figure S5D), following activation to remove residual buffer ions from the gas-phase protein complexes, is negligible, implying that there is no measurable release of the specifically-bound metal ions that provide conformational stability to ConA (Mn^{2+} and Ca^{2+}).

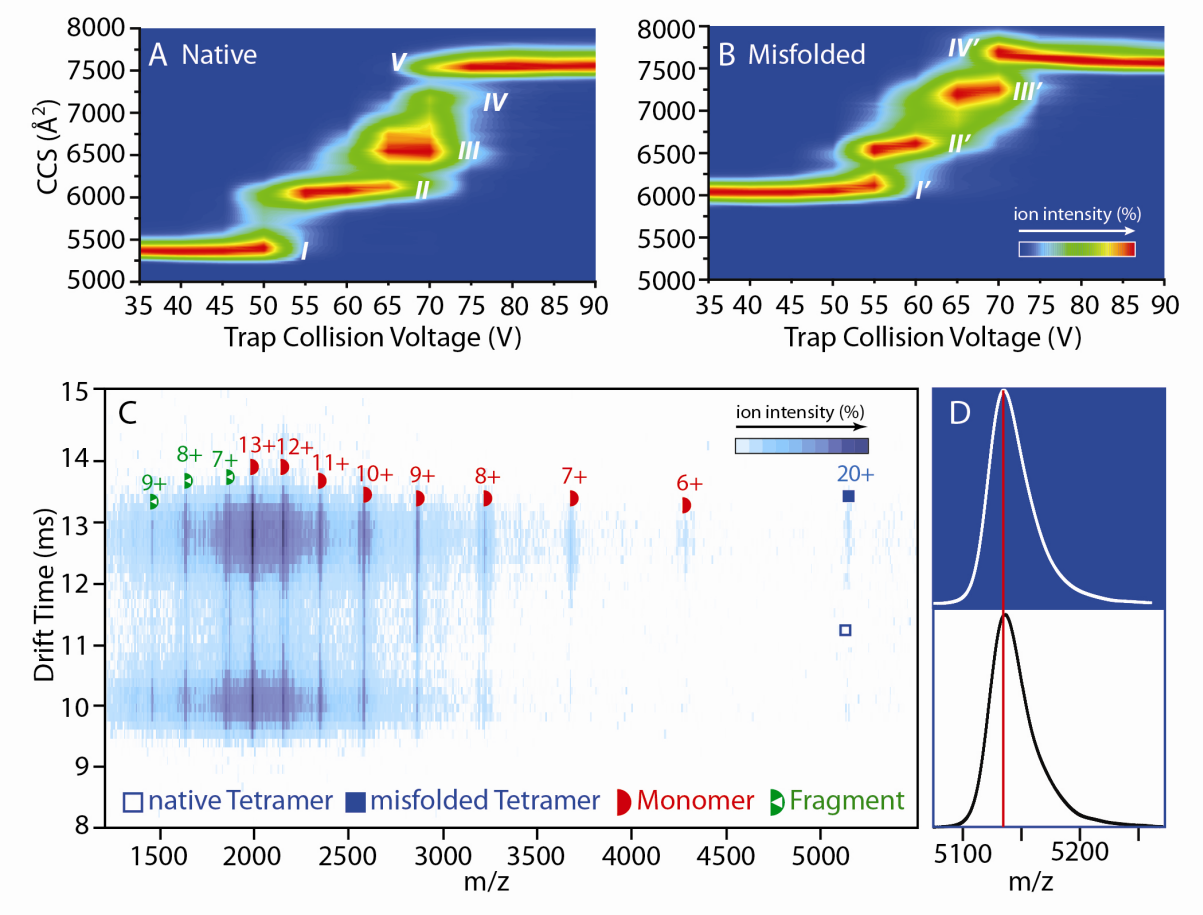

Figure S5. Collisional activation of native concanavalin A tetramer (ConA) and its misfolded form (ConA'). **(A) and (B)** are CIU fingerprint contour plots for 21^+ ConA and ConA' respectively, where trap collision voltage is charted against IM drift time, and ion intensities are denoted by a color-coded axis. The conformational forms observed for ConA (I, II, III, IV and V) and ConA' (I', II', III' and IV') are labeled. **(C)** Drift time versus m/z contour plots obtained for 20^+ ConA and ConA' following post-IM CID. Unfolded monomers and truncated fragments [10] with wide charge state distributions are observed at a collision voltage of 180 V. **(D)** Comparison of MS data for the misfolded (upper) and native-like (lower) forms of 20^+ of ConA tetramer at a transfer collision voltage of 60 V where the majority of residual buffer ions have been removed. A negligible mass difference is recorded (intact mass = 102.7kDa), with red dashed line marked at the m/z of highest abundance (m/z = 5135).

Cation concentration-dependent recovery of ConA' (Figure S6) – Anions recover the misfolded ConA in a fashion nearly identical to solution-phase Hofmeister series (Figure 3A) but cations do not (Figure 3B). Such a discrepancy led us to probe the effect of cations in a detailed manner, focusing on the 21^+ of misfolded ConA tetramer (ConA') created through incubating ConA in an 20%:20% acetic acid:methanol solution, and then adding a series of acetate-based cations at fixed concentrations (Figure S6A). The data agree well with the rank order we have determined previously,[8] and we can quantitatively assess the recovery percentage achieved, calculated as a fraction of native conformer over the sum of all conformational ensembles observed, which is further plotted against the average number of cations bound (Figure S6B). Generally, there is a positive correlation between the % recovery achieved and the amount of cations bound to gas-phase ConA' ions. This highlights the importance of the cations bound to the gas-phase proteins in converting ConA' to ConA. However, we detect a significant difference in the extent of recovery in the cases of Li^+ (grey) and Ba^{2+} (blue), although Li^+ binds in larger numbers to the protein (Figure S6B). As observed previously [8], multiply charged cations (Ca^{2+}, Mg^{2+} and Ba^{2+}), which can form multidentate interactions within proteins in the gas phase, can recover the protein complex more-effectively. It is worth noting that the cation-protein interactions studied here are deemed 'non-specific' because there are no specific binding sites for Mg^{2+} and Ba^{2+} in ConA[11]. Even in our Ca^{2+} data, specific binding is not likely to contribute to the recovery observed, as our Ca^{2+} data mirrors those cations known to be nonspecific ConA binders. This can be confirmed by our concentration-dependent analysis, where larger concentrations of both Ca^{2+} and Mg^{2+} are observed to increase the population of native ConA similarly (Figure S6D and S6E). Previous data has shown that Mg^{2+} cannot interact with the specific metal binding sites within ConA.[13]

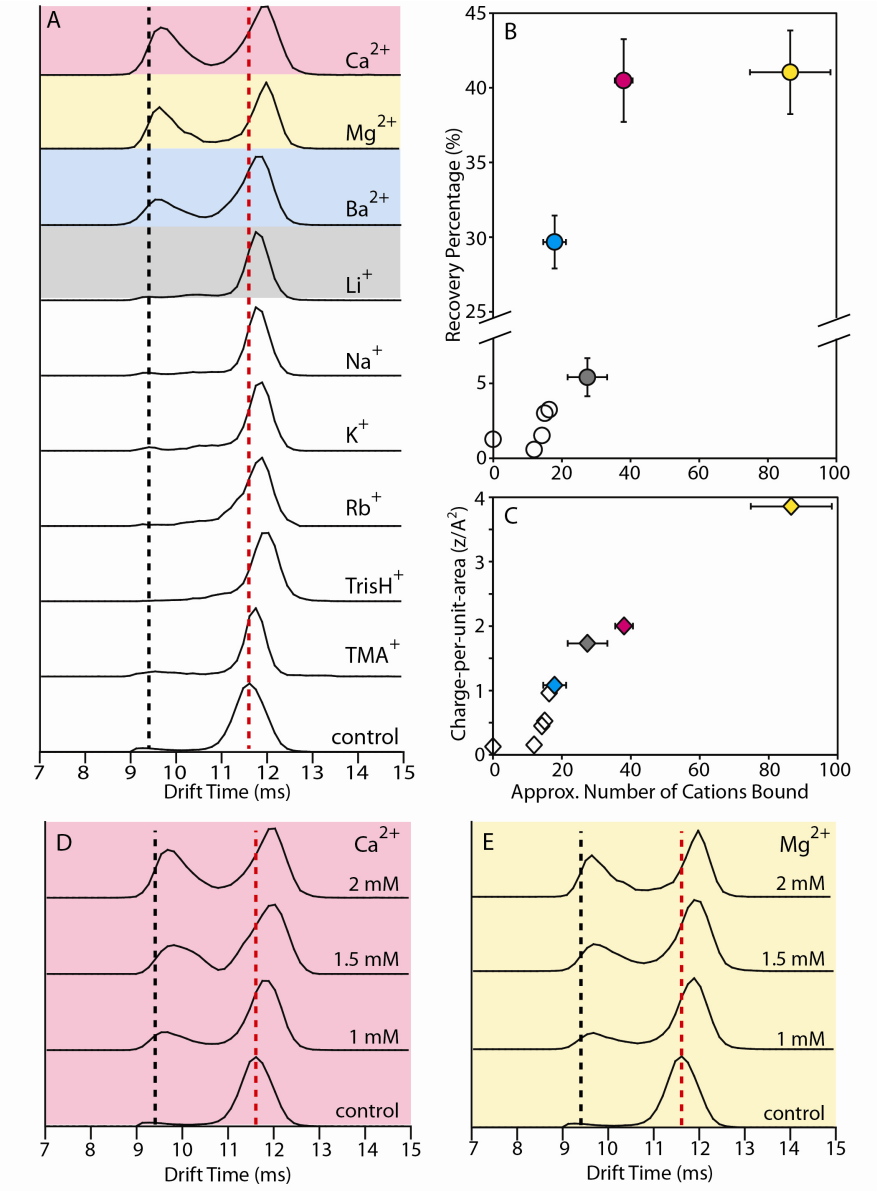

Figure S6. The addition of cations in solution recovers ConA' to ConA in a concentration dependent manner. For all data, black and red dashed lines are inserted in order to guide the eye along drift times corresponding to ConA and ConA' respectively. **(A)** Drift time distributions measured for 21^+ charge state of ConA' tetramer incubated with 9 different acetate-based cations (2 mM) in solution. **(B)** A plot of the average number of cations bound to gas-phase proteins versus % recovery to ConA observed. **(C)** The average number of cations bound to gas-phase ConA' proteins plotted against the charge-per-unit-area of the cations added. A strong correlation is observed between protein-cation binding affinity and the charged area of the added cations. In (B) and (C), four cations are highlighted (red: Ca^{2+}; yellow: Mg^{2+}; blue: Ba^{2+}; grey: Li^+) for discussion in the text. **(D) and (E)** show concentration-dependent analysis, in which drift time distributions measured for 21^+ ConA' incubated with Ca^{2+} and Mg^{2+} are stacked according to the concentration of the added cations.

Verifying recovered ConA' being identical to ConA through collisional activation (Figure S7) – As discussed above, high charge density cations (*i.e.* Mg^{2+} and Ca^{2+}) are able to recover ConA' back to a native-like structure in solution for measurement in the gas phase. To investigate the local structural similarity of recovered ConA' to ConA produced from pure ammonium acetate solutions, CIU fingerprint analysis was performed for 21^{+} ConA' ions recovered through the addition of Mg^{2+} (Figure S7A, red). We note that prior to the addition of Mg^{2+}, IM-MS data indicates that protein in solution was not completely in a disrupted state, containing 44% ConA and 56% ConA'. For a direct comparison, the CIU fingerprinting experiment was also performed for 21^{+} ConA without any disruption, in the presence of an equal Mg^{2+} concentration (2 mM, Figure S7A, black). Cation-mediated CIU fingerprints exhibit strikingly different unfolding pathways when compared with ions produced from 100 mM ammonium acetate buffer[9a]. The two CIU fingerprints recorded share the same unfolding pattern (Figure S7B and C), and are thus indicative of a similar local structure for recovered ConA' and ConA tetramer.

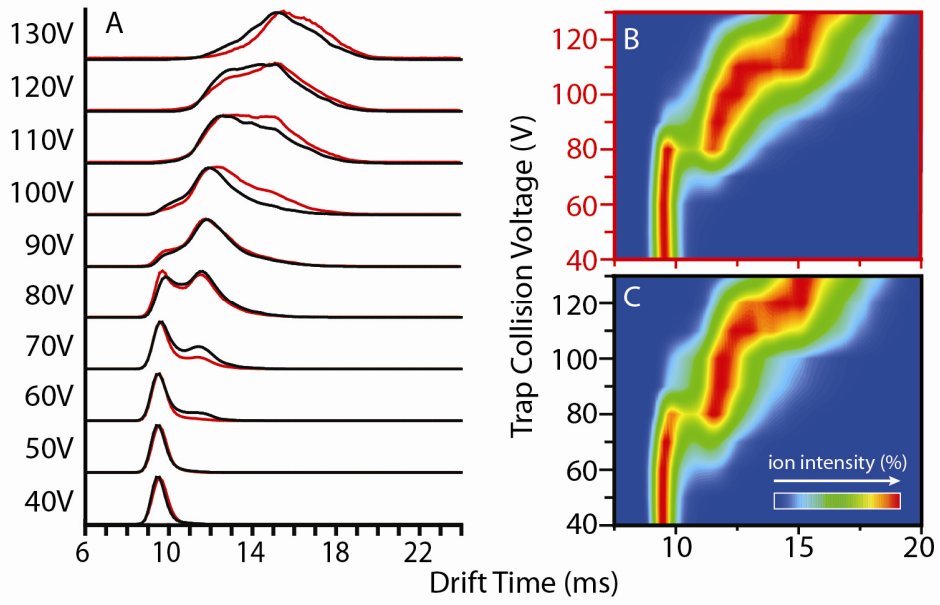

Figure S7. Collisional activation of native ConA and recovered ConA' incubated with added Mg^{2+}. **(A)** The arrival time distributions of 21^{+} charge state of Mg^{2+}-recovered ConA' (red) and Mg^{2+}-incubated ConA (black) acquired at the corresponding trap collision voltages. **(B)** and **(C)** are complete CIU fingerprint contour plots for 21^{+} ions of Mg^{2+}-recovered ConA' and Mg^{2+}-incubated ConA respectively, where ion intensities are denoted by a color-coded axis.

Monitoring the recovery of ConA' to ConA by salts in solution through circular dichroism and differential scanning calorimetry (Detailed Discussion of Figure 4) - For solution experiments designed to monitor anions-based recovery of ConA', we selected three anions (SO_4^{2-}, Cl^- and ClO_4^-) which are regarded as strongly, medium and weakly stabilizing agents respectively in the canonical Hofmeister series. In contrast to our nESI-IM-MS measurements, CD and DSC measurements in solution used salt concentrations high enough to elicit Hofmeister effects in bulk solution (1 M)[12]. As shown in Figure 4A, the absorption band at ~220 nm exhibits greater intensity upon addition of SO_4^{2-} (green) when compared to Cl^- (blue), indicating a more efficient recovery of β-sheet conformation, whereas ClO_4^- has little effect on the rescue of native ConA structure (red). As such, our CD data agree both with the Hofmeister series and our IM-MS data. Further agreement between solution and gas-phase results is discovered when DSC data acquired for ConA' prepared in 10% methanol under weakly-acidic conditions is considered. In the presence of 1 M ammonium sulfate, native ConA stability is recovered, and perchlorate has no influence on protein stability (Figure 4C), also in agreement with IM-MS data. We note that solution pH changes by <0.2 when SO_4^{2-} and ClO_4^- are present in our experiments. Thus, it is likely that the addition of SO_4^{2-} converts ConA' to ConA using the Hofmeister effect, rather than shifts in pH and buffer capacity. The recorded thermal unfolding transition for SO_4^{2-} containing ConA solutions results in a T_m shift from ~64 °C to ~84 °C, the latter a characteristic value for native ConA. Conversely, the DSC trace for ClO_4^--incubated ConA' exhibits three main features all with depressed stabilities (T_m: 56, 64, 70 °C), indicative of a disrupted ConA structure. Taken together, anion data mirror our IM-MS measurements, and the expected Hofmeister series, precisely (Figure 3A).

Surprisingly, our CD and DSC data for added cations in solution follows an inverse Hofmeister series. For example, Mg^{2+} is a protein destabilizer in the canonical Hofmeister series, but acts to dramatically recover ConA structure (Figure 4B) and thermal stability (T_m: ~84 °C, Figure 4C), whereas $N(CH_3)_4^+$, an expected stabilizer, does not act to alter ConA conformation or stability in a measurable way. We attribute this result to the relatively negatively charged ConA surface under our conditions (pI=5.43) and the relatively low concentration for cations added (1 M), as has been previously observed for positively charged protein and anions in low abundance (<300 mM)[12-13]. The discrepancy between the threshold concentrations needed to illicit reversed Hofmeister effects observed for anions and cations is likely due to the enhanced ability of anions to alter water structure, in general, which typically leads to their enhanced Hofmeister effect when compared to equivalent cations for experiments carried out in solution.[12] While this general result maps well onto our IM-MS dataset, the general agreement achieved between our IM-MS data and a previous survey of gas-phase only protein stability

measurements provides, arguably, a better fit for the cation mediated stability shifts observed in this report.[14] For example, Li^+ exhibits the poorest ability to stabilize ConA in solution, and predictions made from a reversed Hofmeister point of view would typically place this cation as an intermediate destabilizer. It is therefore reasonable to conclude that a combined effect exists where cations are able to recover ConA' in solution and also prevent this rescued form from converting to an elongated quaternary structure upon desolvation by tethering the flexible regions of the protein complex during the transmission into the gas phase. In addition, in our reports, as in our data here, stronger shifts in protein stability were observed when multiply-charged salt additives were used versus those having a single charge, which we interpreted as related to the ability of such salts to form direct, multi-dentate interactions with the protein.

Calcium nonspecifically binding to ConA' (Figure S8) – As discussed above, we observe no evidence for the release of specifically-bound metal ions from ConA upon conversion to ConA'. Appropriately bound Mn^{2+} and Ca^{2+} ions are required for sugar binding, and we have observed that samples containing significant amounts of disrupting agents can still bind sugars known to be tight binders to native ConA by MS (data not shown). Furthermore, the number of divalent metal ions adhered to the protein far exceeds the known binding stoichiometry of the native protein, further indicating that a non-specific Hofmeister effect is primarily operative in the stability shifts observed in our data. For example, MS data collected and compared between ConA' and ConA' incubated with 2 mM Ca^{2+} (Figure S8) displays a mass shift of 1.8 kDa. If it is assumed that all of the excess mass recorded is due to Ca^{2+} binding (an assumption that is supported by much control data for smaller protein systems)[14], then a binding stoichiometry close to 1:45 results, which is far above the 4 expected binding sites on ConA.

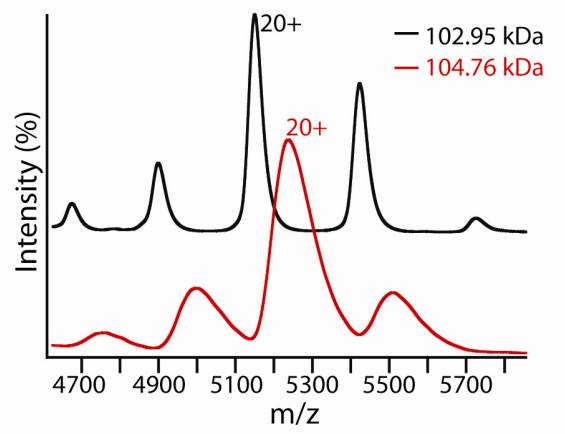

Figure S8. Nano-electrospray ionization (nESI) mass spectra of ConA' (5 µM) generated with 20%:20% HAc: MeOH and the same ConA' (5 µM) further incubated with 2 mM Ca^{2+}, colored by black and red, respectively. The 2 spectra were obtained using identical instrumental conditions. The molecular weight of ConA' and Ca^{2+}-bound ConA' is indicated (kDa).

Possible mechanisms driving the CCS change in ConA tetramer, dimer and monomer (Figure S9) - Based on our IM-MS (Figures 1, S2, S3, S4) and CD/DSC (Figure 2) data, we have evaluated several potential mechanisms that explain the appearance of ConA' under some solution conditions. A pictorial summary of these are shown in Figure S9. In one scenario, the disruption of key H-bonds within the ConA dimer interface loosens it to produce ConA' in solution (Figure S9A). While this engenders misfolding at the interface, the re-arranged tertiary structure is compact at the dimer scale and serves only to prevent the dimer-dimer interdigitation observed in native ConA. Monomers, once released from the dimer undergo unfolding at their now exposed monomer-monomer interfaces, producing a range of unfolded structures. We treat each of these as equilibrium based (reversible) processes. In a related mechanism (Figure S9B) the ConA dimer-dimer interface is still loosened to create ConA', but dramatic changes in protein size occur only upon desolvation. This holds for monomers as well, where destabilized monomer units undergo dramatic unfolding only in the absence of solvent. In a final scenario considered (Figure S9C), monomer building blocks of ConA are destabilized in solution, leading to asymmetric unfolding of the tetramer in the gas phase to produce ConA'. Again, similar forces influence the monomers in the gas-phase, but not the dimers, potentially due to differential amounts or densities of charge deposited on each ion surface during nESI.

The first scenario (Figure S9A) has the strongest agreement with all of our data, in that our CD/DSC data show that large structure and stability changes occur in bulk solution. In the other two mechanisms shown in Figure S9, protein structure changes occur primarily in the gas-phase. Currently, however, we cannot map the magnitude of the structure changes observed in our solution-phase datasets to those obtained by IM-MS, therefore it is still possible that some portion of the structural change observed by IM-MS occurs as a direct result of desolvation. The third model shown (Figure S9C) invokes assymetric unfolding of a single subunit to form ConA'. The gas-phase is the only environment where such assymetric unfolding is thought to take place, and since our CD/DSC suggests that substaintial unfolding/misfolding takes place in solution, that makes this mechanism less likely than the other two shown. If cation/anion recovery (Figures 3 and 4) and CIU fingerprinting (Figure S5A and S5B) data are included in our analysis, the model shown in Figure S9C becomes even less likely. These data invoke clear methods of recovery that take place in bulk solution, and critically show that the ConA' monomers

that comprise the tetramer undergo similar unfolding to those in ConA, suggesting that assyemtric unfolding has yet to take place in ConA' prior to collisional activation. Cation-based stabilization, while generally agreeing with results found for ConA in bulk solution shown in Figure 4, also agree with previous gas-phase stability measurements of protein-cation complexes, thus potentially lending more-credence to the importance of the model shown in Figure S9B.[14] Therefore, some combination of the models shown in Figures S9A and S9B explain (and our consistent with) all of the data we present in this report.

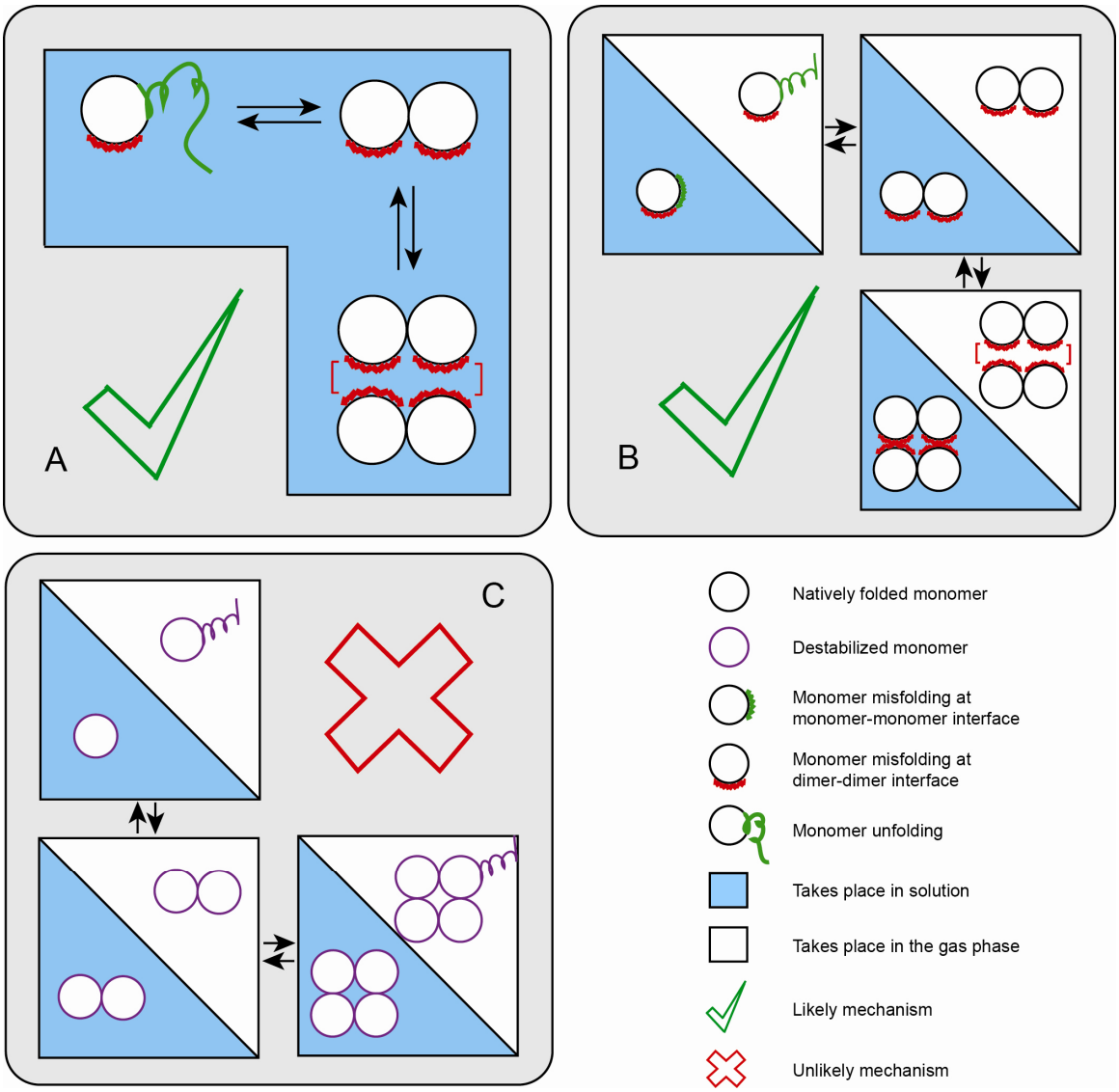

Figure S9. A schematic diagram showing three possible mechanisms that describe the formation of ConA' from ConA. See the legend included and the text for a detailed description.

Comparison of ConA salt stabilization to Literature Hofmeister effects – There are a number of different sets of results that describe the differential affects of salts on the stability and solubility of solutes in solution. For example, Randall and Failey studied the ability of different salts to solublize a range of different solutes, including gases (H_2, N_2, O_2, CO_2, NH_3, He, etc.) and other non electolytes (I_2, nitrobenzaldehyde, etc.), developing a rank order for their influence with significant differences to Hofmeister's original order (where primarily protein solutes were studied).[15] For Anions, Randall and Failey's rank order is: $SO_4^{2-} > ClO_4^- > Cl^- > CH_3COO^- > Br^-, I^- > NO_3^-$ and Hofmeister's original rank order is: $SO_4^{2-} > H_2PO_4^- > F^- > Cl^- > Br^-, NO_3^- > ClO_4^-$.[15] While we, at no point, attempted a strict quantification of the stabilities enhancements afforded by anions to ConA, our data shown in Figure 3 clearly is more highly-correlated with Hofmeister's original rank order than with the Randall and Failey order. For example, the Randall and Failey order classifies ClO_4^- as a relative stabilizer, where as both our data and the Hofmeister order make the opposite assessment. Minor disagreements between our anion data and the canonical Hofmeister series can be seen in the relative positions of SO_4^{2-} and $H_2PO_4^-$, which are reversed in our data, but still both classified as strongly stabilizing. This small discrepancy is unlikely to be significant, and we conclude that our data and the Hofmeister series are strongly correlated. This result is not surprising, given the origins of the Randall and Failey rank order in the study of simple solutes, many of which can be treated as non-electrolytes. Recent data have strongly indicated that the charge and chemical nature of the solute is a key determining factor in the salt-based stabilization effects observed.[12]

Cation effects are less-studied in the Hofmeister community, as they are usually diminished in strength relative to their anionic analogs.[12] The typical rank order associated with the Hofmeister effect for protein solutes is: $NH_4^+ > K^+ > Na^+ > Li^+ > Mg^{2+} > Ca^{2+}$, while the Randall and Failey rank order is: $Na^+ > K^+ > Li^+ > Ca^{2+} > Mg^{2+} > NH_4^+$.[15] Neither our IM-MS nor our DSC/CD data agrees with either of these rank orders, despite their differences. Strongest agreement is found to a reversed form of the Hofmeister rank order, or with our previous rank order that measures the stability of protein-cation complexes in the absence of solvent.[14] While a reversed Hofmeister series agrees well with our IM-MS data, discrepancies exist when compared with our DSC/CD data. The key difference between the two datasets is Li^+, which is intermediately stabilizing in our IM-MS data, but destabilizing in our DSC/CD data. However, overall, we observe good agreement between our solution and gas-phase datasets. Reversed Hofmeister effects have been observed in some instances in the context of anions in cases where the solute bears charges of opposite polarity.[16] The pI of ConA is 5.4, which give the protein an overall negative charge at pH 7, potentially serving to drive to the reversal of the canonical Hofmeister series both in solution and reflected in our IM-MS data for ConA.

References:

[1] Y. Zhong, S.-J. Hyung, B. T. Ruotolo, *Analyst* **2011**, *136*, 3534-3541.

[2] T. M. Annesley, *Clin. Chem.* **2003**, *49*, 1041-1044.

[3] a) B. T. Ruotolo, J. L. P. Benesch, A. M. Sandercock, S. J. Hyung, C. V. Robinson, *Nat. Protoc.* **2008**, *3*, 1139-1152; b) H. Hernandez, C. V. Robinson, *Nat. Protoc.* **2007**, *2*, 715-726.

[4] a) M. F. Bush, Z. Hall, K. Giles, J. Hoyes, C. V. Robinson, B. T. Ruotolo, *Anal. Chem.* **2010**, *82*, 9557-9565; b) T. Taverner, H. Hernandez, M. Sharon, B. T. Ruotolo, D. Matak-Vinkovic, D. Devos, R. B. Russell, C. V. Robinson, *Accounts Chem. Res.* **2008**, *41*, 617-627.

[5] J. L. P. Benesch, B. T. Ruotolo, D. A. Simmons, C. V. Robinson, *Chem. Rev.* **2007**, *107*, 3544-3567.

[6] A. T. Iavarone, E. R. Williams, *J. Am. Chem. Soc.* **2003**, *125*, 2319-2327.

[7] a) A. Naeem, A. Khan, R. H. Khan, *Biochem. Biophys. Res. Commun.* **2005**, *331*, 1284-1294; b) S. Sinha, N. Mitra, G. Kumar, K. Bajaj, A. Surolia, *Biophys. J.* **2005**, *88*, 1300-1310.

[8] J. N. Sanders, S. A. Chenoweth, F. P. Schwarz, *J. Inorg. Biochem.* **1998**, *70*, 71-82.

[9] a) L. J. Han, S. J. Hyung, B. T. Ruotolo, *Faraday Discuss.* **2012**, *160*, 371-388; b) J. Freeke, M. F. Bush, C. V. Robinson, B. T. Ruotolo, *Chem. Phys. Lett.* **2012**, *524*, 1-9.

[10] L. Han, B. T. Ruotolo, *Int. J. Ion Mobility Spectrom.* **2013**, *16*, 41-50.

[11] M. Shoham, A. J. Kalb, I. Pecht, *Biochemistry* **1973**, *12*, 1914-1917.

[12] Y. J. Zhang, P. S. Cremer, *Annu. Rev. Phys. Chem.* **2010**, *61*, 63-83.

[13] Y. J. Zhang, P. S. Cremer, *Proc. Nat. Acad. Sci. U.S.A.* **2009**, *106*, 15249-15253.

[14] L. J. Han, S. J. Hyung, B. T. Ruotolo, *Angew. Chem.-Int. Edit.* **2012**, *51*, 5692-5695.

[15] P. Lo Nostro, B. W. Ninham, *Chem. Rev.* **2012**, *112*, 2286-2322.

[16] Y. J. Zhang, P. S. Cremer, *Curr. Opin. Chem. Biol.* **2006**, *10*, 658-663.